APPLIED GEOPHYSICS, Vol.15, No.2 (June 2018), P. 299–310,11 Figures.
DOI:10.1007/s11770-018-0679-4

Numerical analysis of seismic wave propagation in fluid-saturated porous multifractured media*

Guo Gui-Hong[1], Yan Jian-Ping[2], Zhang Zhi♦[3], José Badal[4], Cheng Jian-Wu[5], Shi Shuang-Hu[6], and Ma Ya-Wei[1]

Abstract: Elastic wave propagation and attenuation in porous rock layers with oriented sets of fractures, especially in carbonate reservoirs, are anisotropic owing to fracture sealing, fracture size, fracture density, filling fluid, and fracture strike orientation. To address this problem, we adopt the Chapman effective medium model and carry out numerical experiments to assess the variation in P-wave velocity and attenuation, and the shear-wave splitting anisotropy with the frequency and azimuth of the incident wave. The results suggest that velocity, attenuation, and anisotropy vary as function of azimuth and frequency. The azimuths of the minimum attenuation and maximum P-wave velocity are nearly coincident with the average strike of the two sets of open fractures. P-wave velocity is greater in sealed fractures than open fractures, whereas the attenuation of energy and anisotropy is stronger in open fractures than sealed fractures. For fractures of different sizes, the maximum velocity together with the minimum attenuation correspond to the average orientation of the fracture sets. Small fractures affect the wave propagation less. Azimuth-dependent anisotropy is low and varies more than the other attributes. Fracture density strongly affects the P-wave velocity, attenuation, and shear-wave anisotropy. The attenuation is more sensitive to the variation of fracture size than that of velocity and anisotropy. In the seismic frequency band, the effect of oil and gas saturation on attenuation is very different from that for brine saturation and varies weakly over azimuth. It is demonstrated that for two sets of fractures with the same density, the fast shear-wave polarization angle is almost linearly related with the orientation of one of the fracture sets.
Keywords: Fracture, fluid, wave, velocity, attenuation, anisotropy, polarization.

Introduction

Fractures in sedimentary rocks play an important role in oil and gas reservoirs. The subsurface structure is affected by multiple tectonic movements that create sets of aligned fractures at scales ranging from millimeters to meters (Crampin et al., 1978, 1985, 1994, 2014; Liu et

Manuscript received by the Editor December 13, 2017; revised manuscript receivered January 24, 2018.
*This study was supported by the National Natural Science Foundation of China Rsearch (Nos. 41674046, 41440030, and 41574078) and the Fundamental Research Funds for the Central Universities of Lanzhou university (No. lzujbky-2015-175).
1. Lanzhou University & The Key Laboratory of Mechanics on Disaster and Environmental in Western China, Lanzhou 730000, China.
2. Lanzhou University & School of Earth Sciences, Lanzhou 730000, China.
3. School of Earth Science, Guilin university of science and technology, Guilin 541004, China.
4. Physics of the Earth, Sciences B, University of Zaragoza, Pedro Cerbuna 12, 50009 Zaragoza, Spain.
5. Lanzhou Institute of Seismology, China Earthquake Administration, Lanzhou 730000, China.
6. BGP International, CNPC, Zhuozhou 072751, China.
♦Corresponding author: Zhang Zhi (Email: zhangzhi@glut.edu.cn)

al., 2006) and are filled with fluid or are fluid-saturated. Mid-sized fractures are the main reason for the seismic anisotropy in oil and gas fields (Liu et al., 1993). Fractures obviously change the mechanical properties of rocks (Schoenberg, 1999) and can cause seismic anisotropy (Hudson et al., 1996; Pointer et al., 2000; Chapman, 2003, 2009; Liu et al., 2006). Several studies on seismic anisotropy have been conducted in fractured media at single scales (Hudson et al., 1996; Pointer et al., 2000; Jakobsen, 2004; Shi et al., 2007; Agersborg et al., 2009; Guo et al., 2013).

Variation of seismic anisotropy with frequency is observed in fractured and porous media (Liu et al., 2001, Maultzsch et al., 2003). The analysis of field data suggests that the frequency dependence of the seismic anisotropy provides information about the fluid saturation and fracture scale in fractured reservoirs (Maultzsch et al., 2007a, 2007b). The velocity and attenuation of the seismic waves and the seismic anisotropy of the medium vary with frequency (Batzle et al., 2006; Liu et al., 2012). Considering mid-sized fractures and pores, Chapman (2003, 2009) studied effective medium models for multiscale fracture sets with different azimuths. Hao and He (2013) proposed a standard linear model to represent Chapman's frequency-dependent anisotropy. In effective medium models, it is assumed that pressure differences are due to fluid flow between fractures and pores. An important aspect of rock physics is calculations based on pores with the same radius microcracks, and mid-scale fractures, and the decrease of the dependence of the parameters of the medium with fracture aspect radio.

The Chapman (2009) effective medium model is for viscoelastic anisotropic materials. The theory of wave propagation in viscoelastic anisotropic media was studied systematically by Borcherdt (2009) and Carcione (2015), and ray propagation in viscoelastic anisotropic media has been studied by Cerveny and Psencik (2001, 2009). Recently, Hao and Alkhalifah (2017a, 2017b) proposed the acoustic eikonal equations governing the P-wave complex-valued traveltimes in viscoelastic anisotropic media. For more details about viscoelastic waves and ray propagation, the reader is referred to the original papers.

In this study, we study the seismic wave propagation in fluid-saturated porous multifractured media considering fracture-related features, such as sealing, size, density, filling fluid, and strike of the fractures. Basically, we perform several numerical experiments aimed to assess the variation of the P-wave velocity, inelastic attenuation, and shear-wave splitting anisotropy for a wide frequency band and the azimuthal angle of the wave. The study of seismic wave propagation in porous and fractured media has not only theoretical value but also has great practical significance in seismic exploration.

Elastic parameters in multifractured media

The frequency-dependent elastic tensor in multifractured media is linearly expressed as (Chapman, 2003, 2009)

$$C_{ijkl}(\omega) = C^0_{ijkl} - \varphi C^p_{ijkl}(\omega) - \varepsilon_1 C^{f_1}_{ijkl}(\omega) - \varepsilon_2 C^{f_2}_{ijkl}(\omega), \quad (1)$$

where ω is the angular frequency and φ is the porosity, C^0_{iikl} is the constant elastic tensor, $C^p_{ijkl}(\omega)$ is the elastic tensor of the pores, $C^{f_1}_{ijkl}(\omega)$ and $C^{f_2}_{ijkl}(\omega)$ are two elastic tensors in correspondence with two sets of fractures, and ε_1 and ε_2 are the fracture densities (see appendix A). Equation (1) shows the contribution of porosity to the elastic tensor for two sets of fractures. Ignoring the elastic interaction between fractures and pores leads to a first-order elastic tensor with respect to porosity and fracture density. The two sets of fractures correspond to two time-scale factors that are related to the scale of the fracture sets and the macroscale flow owing to fractures. Each of the elastic constants is related to the fracture size by the characteristic time-scale factors τ_1 and τ_2 ($\tau_f = \frac{8l(1-\upsilon)(1+K_c)}{3\mu}\left(\frac{\eta}{k}\right)a_f$), in correspondence with the two fracture sizes. The model can be used to estimate the fracture size from the observed anisotropy (Liu et al., 2000; Maultzsch et al., 2003).

Velocity, attenuation, and anisotropy

In this section, we address the propagation characteristics of a plane wave in a multifractured medium based on the Christoffel equation (Fedorov, 1968; Chapman, 2003, 2009). The wave equation without a body force is

$$\rho \frac{\partial^2 u_i}{\partial t^2} - c_{ijkl} \frac{\partial^2 u_k}{\partial x_j \partial x_l} = 0. \quad (2)$$

The plane wave harmonic solution is (Aki and Richards, 1980)

$$u_k = U_k \exp\left\{\frac{i\omega}{V}[\vec{n}\cdot\vec{x} - Vt]\right\}, \quad (3)$$

where U_k is the displacement amplitude, $\vec{x} = (x, y, z)^T$ is the position vector, $\vec{n} = (\sin\theta\cos\varphi, \sin\theta\sin\varphi, \cos\theta)^T$ is the propagation direction of the plane wave, θ is the polar angle, φ is the azimuthal angle, ω is the angular frequency, and V is the phase velocity. Substituting equation (3) into the wave equation (2), we obtain

$$\begin{bmatrix} G_{11}-\rho V^2 & G_{12} & G_{13} \\ G_{21} & G_{22}-\rho V^2 & G_{23} \\ G_{31} & G_{32} & G_{33}-\rho V^2 \end{bmatrix} \begin{bmatrix} U_1 \\ U_2 \\ U_3 \end{bmatrix} = 0, \quad (4)$$

where $G_{ik} = c_{ijkl} n_j n_l$ depends on the elastic constants of the medium and the propagation direction of the plane wave. The solution of the Christoffel equation gives rise to the phase velocity (V) and polarization vector (U). The inverse of the quality factor is

$$Q^{-1} = \frac{\mathrm{Im}(V^2)}{\mathrm{Re}(V^2)}. \quad (5)$$

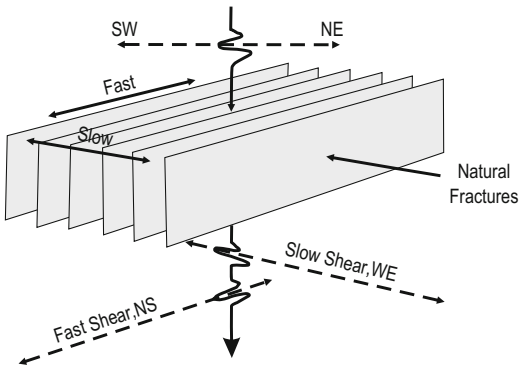

Fig.1 Shear-wave splitting in a fractured medium.

When a shear wave travels through an anisotropic medium, it is divided into two waves (shear-wave splitting). One wave is polarized approximately parallel to the strike of the fractures (S1) and is called the fast wave, and the other is polarized approximately perpendicular to the strike of the fractures (S2) and is called the slow wave (Figure 1). The splitting anisotropy is defined as (Kraut, 1963)

$$D(v) = \frac{V_{S1} - V_{S2}}{V_{S1}} \times 100\%, \quad (6)$$

where V_{S1} and V_{S2} denote the S1-wave and S2-wave velocity, respectively.

Assuming that the fast shear-wave polarization vector is denoted by U_1, U_2 and U_3, the fast-wave polarization direction ϕ_{fast} is defined by the expression (Tsvankin, 2001)

$$\tan(\phi_{fast}) = \frac{U_2}{U_1}. \quad (7)$$

The stiffness parameters polarization vector is obtained from equations (1) to (7), and all these quantities, i.e., wave velocity, quality factor, splitting anisotropy, and polarization direction, depend on the frequency, fracture size, and orientation.

Numerical experiments

In the following examples, we consider two sets of vertical fractures. The fluid properties are listed in Table 1. The model parameters are as follows: P-wave velocity is 6475 m/s; S-wave velocity is 3340 m/s; density is 2600 kg/m^3; porosity is 8%; grain size is 200 μm; and the aspect ratio is 0.0001. The stiffness parameters are calculated according to equation (A-35) of Appendix A. The seismic velocity, the inverse of the quality factor (attenuation), splitting anisotropy, and fast-wave polarization direction are obtained from the Christoffel equation (4).

Table 1 Properties of the filling fluid in the calculations

	Brine	Oil	Gas
Velocity (m·s^{-1})	1710	1250	620
density (kg·m^{-3})	1100	800	65
viscosity (Pa·s)	0.001	0.02	2×10^{-5}
Time scale τ_f (s)	0.1	2.0	0.002

Opening or sealing of fractures

The results suggest that the P-wave velocity is greater in sealed fractures than open fractures (Figure 2). The attenuation and splitting anisotropy are lower in sealed fractures than open fractures. In the low-frequency band, the P-wave velocity is low; however, the splitting anisotropy is high because fluid flow compresses the fractures. In the high-frequency band, owing to the unbalanced fluid pressure, the medium is elastic and thus the splitting anisotropy is low. In the moderate-frequency band, there is high attenuation because the dispersion for open fractures is steep. In any case, the

effect of attenuation on sealed fractures can be ignored.

We perform a similar numerical experiment to show the variation of velocity, attenuation, and splitting anisotropy with azimuth (Figure 3). The velocity in a sealed fracture is higher than in an open fracture in the test range (Figure 3a). The results suggest that the P-wave velocity changes with the azimuth in the opposite sense to attenuation (Figure 3b). The velocity (Figure 3a) and anisotropy (Figure 3c) data reach maxima around azimuth 110º, which is the average azimuth for the two types of fractures. The velocity and anisotropy maxima, and the attenuation minimum in sealed fractures are found near 90°, which is the orientation of the open fractures. The maximum P-wave velocity corresponds (Figure 3a) to the minimum attenuation (Figure 3b). Based on these results, it is possible to use the symmetry between velocity and attenuation to determine if the fracture systems are open or sealed. In addition, the maximum velocity or minimum attenuation could be used to determine the average direction of the open fractures.

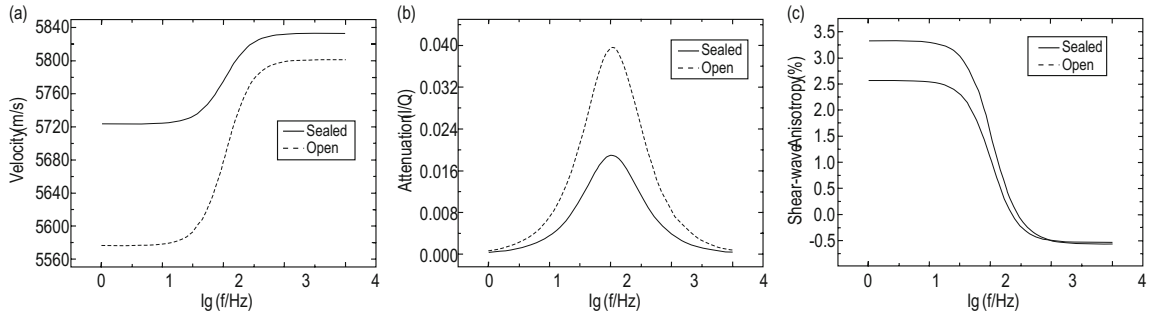

Fig. 2 P-wave velocity (a), inelastic attenuation (b), and shear-wave splitting anisotropy (c) versus frequency.
The numerical simulations are performed for polar and azimuthal angles of 30°, and two sets of 10-cm-sized identically aligned fractures; some open, with brine and 90° strike, and others sealed and striking 130°.

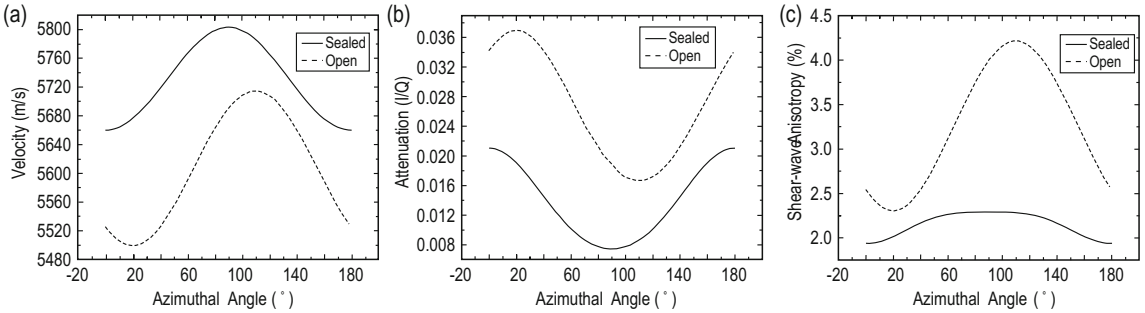

Fig.3 P-wave velocity (a), inelastic attenuation (b), and shear-wave splitting anisotropy (c) versus azimuth.
The numerical simulations are performed for polar angle of 40° and two sets of 10-cm-sized identical aligned fractures; some open, with brine and striking 90°, and others sealed and striking 130°.

Fracture size

Figure 4a shows that the greater the difference in size of the two sets of fractures is, the more complex the P-wave dispersion variation with frequency is. At low frequencies, the velocity and splitting anisotropy data are shown for the 1:1 and 1:10 scales. At high frequencies, the corresponding velocity and splitting anisotropy for the 1:100 and 1:1000 scales are very close. At the 1:1 and 1:10 scales, and in both scales the P-wave velocity is nearly the same at low frequencies, whereas the velocity increases fast at moderate and high frequencies for both scales; nevertheless, the P-wave dispersion is always high for fractures of the same size (1:1). The attenuation and dispersion are high, and the splitting anisotropy is low at high frequencies. There are two attenuation peaks when the scale of the second set of fractures becomes as small as the scale of the first set of fractures. The frequencies of the first peak are near each, and the second peak is associated with high frequency.

The P-wave velocity and anisotropy data coincide for 1:10 and 1:100 along the entire azimuth range (Figs. 5a, 5c), whereas the attenuation (Figure 5b) differs

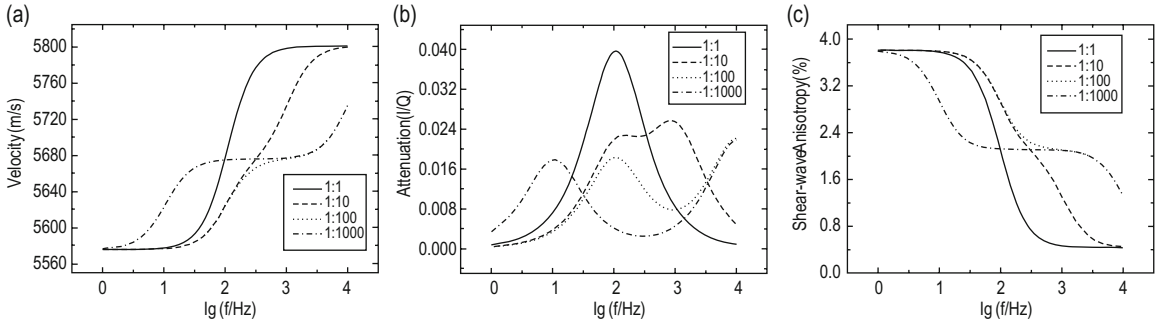

Fig.4 P-wave velocity (a), inelastic attenuation (b), and shear-wave splitting anisotropy (c) versus frequency.
The numerical simulations are performed for polar and azimuthal angles of 30°, and two sets of identical aligned fractures striking 90° and 130°, with brine and for different fracture-size scales (0.1:0.1, 0.1:0.01, 0.1:0.001, 1:0.001).

depending on the scale. All data, however, have minima at intermediate azimuth and are progressively displaced to higher azimuth with increasing scale. The azimuth of the maximum velocity or the minimum attention depends on the average orientation of the fracture sets (Figure 5b). Small fractures have lesser effect on the wave propagation attenuation (Figure 5b) and the average orientation of the two sets of fractures, as expected. At scale 1:1000, the anisotropy is lower and significantly different than in the other cases (Figure 5c), in correspondence with the lesser internal friction (Figure 5b).

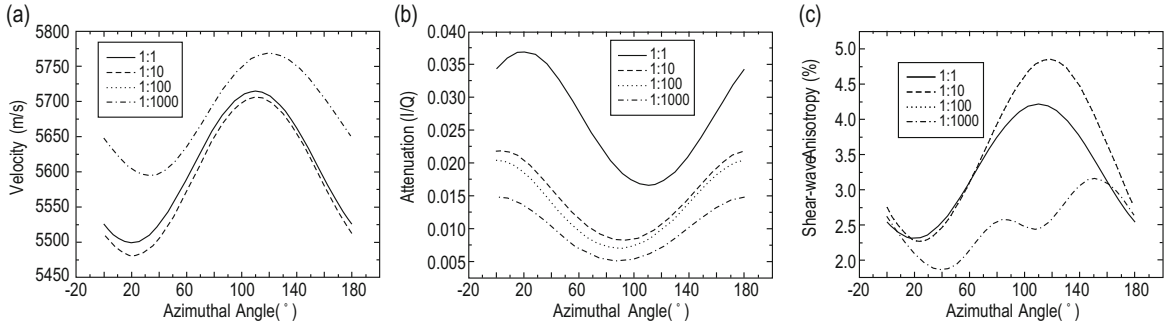

Fig.5 P-wave velocity (a), inelastic attenuation (b), and shear-wave anisotropy (c) versus azimuth.
The numerical simulations are performed for polar angle of 40°, and two sets of identical aligned fractures striking 90° and 130°, filled with brine, and for different scales (0.1:0.1, 0.1:0.01, 0.1:0.001, 1:0.001).

Fracture density

In general, despite the high velocity values for density scale of 1:1 and the low values for the other density scales, the P-wave dispersion varies similarly (Figure 6a) , i.e., for a change of 0.05 (1:2.5) or 0.1 (1:5) in fracture density. In any case, the velocity increases at higher frequencies and the increase is steeply linear at mid frequencies (around 100 Hz). Conversely, the attenuation of energy is lower in the first case, i.e., for the same fracture density (1:1), and more pronounced at 100 Hz (Figure 6b). The attenuation is symmetric with respect to frequency (Figure 6b) and increases when there is notable difference in fracture density (1:2.5, 1:5) and decreases for similar fracture densities (1:1). The anisotropy is high when there are large differences in fracture density (1:2.5, 1:5) at low frequencies, but it is the same for the fracture density (1:1) at high frequencies (Figure 6c).

Figure 7 shows the P-wave velocity versus azimuth, in which pronounced variation is observed throughout the entire interval of the azimuthal angle and for fracture densities of 0.05 (1:2.5) and 0.1 (1:5). The maximum P-wave velocity shifts from 110º to 120º with density. Attenuation changes in the opposite to velocity (Figure 7b), with a slight shift of the minimum towards greater azimuths as the fracture densities change. The anisotropy variation is bell-shaped (Figure 7c), with maxima between 110º and 120º, and is greater for high fracture density differences. In comparison to fracture size and the opening or sealing of the fractures, fracture density has the biggest effect on anisotropy.

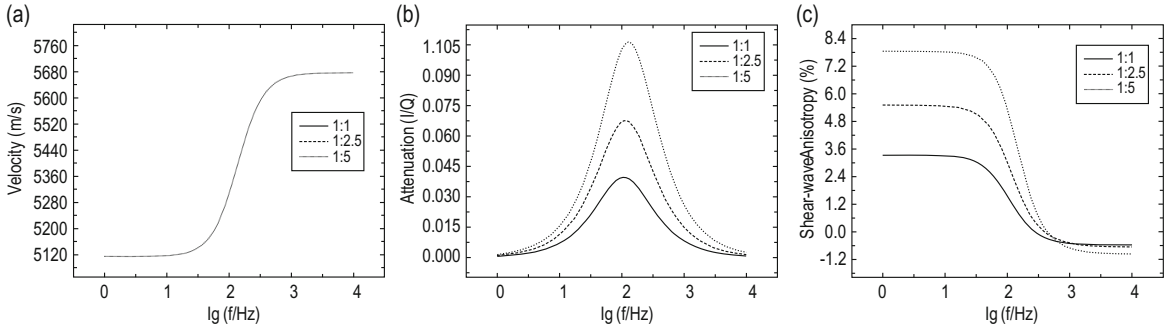

Fig.6 P-wave velocity (a), inelastic attenuation (b), and shear-wave anisotropy (c) versus frequency.
The numerical simulations are performed for polar and azimuthal angles of 30°, and two sets of 10-cm-sized identical aligned fractures striking 90° and 130° for different density scales (0.02:0.02, 0.02:0.05, 0.02:0.1).

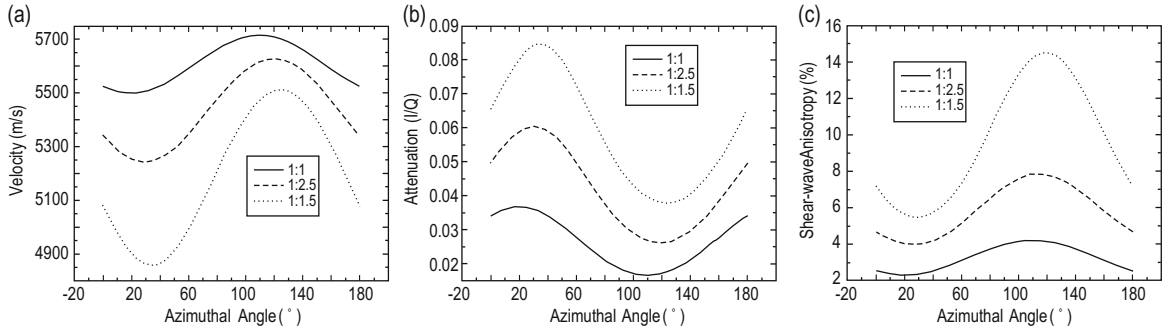

Fig.7 P-wave velocity (a), inelastic attenuation (b), and shear-wave anisotropy (c) versus azimuth.
The numerical simulations are performed for polar angle of 40°, and two sets of 10-cm-sized identical aligned fractures striking 90° and 130° for different density scales (0.02:0.02, 0.02:0.05, 0.02:0.1).

Filling fluid

Filling fluids have different viscosities and different characteristic frequencies. Therefore, the characteristic frequencies of the attenuation peaks are also different. In any case, the anisotropy is lower for oil and brine (in this order) than for gas. In both set of fractures, the decreasing splitting anisotropy moves to high frequencies. In general, the type of the filling can be distinguished by the attenuation peak around frequency band rang.

Looking at the P-wave velocity variation with azimuthal angle (Figure 9a), we see smooth changes with azimuth for oil and gas, and a stronger variation for brine, even though the highest velocity values for oil and gas (in this order) are clearly above the velocity values for brine. The P-wave velocity peaks for oil and gas occur at about 110º, whereas for brine it occurs are at 120º. The most pronounced variation and

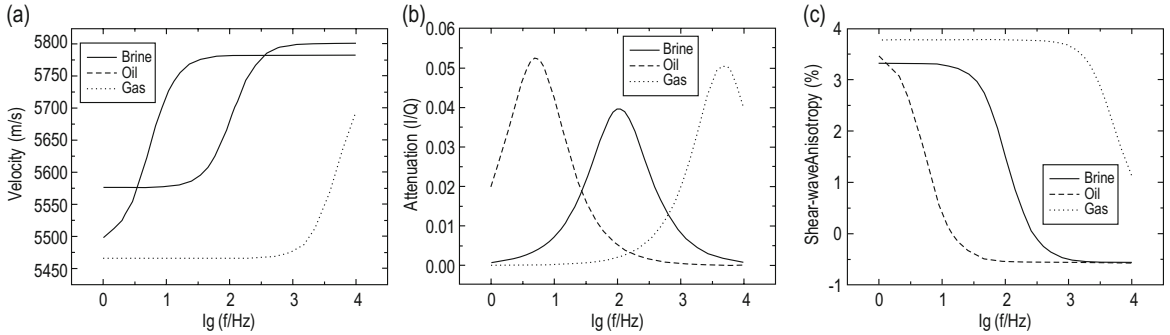

Fig.8 P-wave velocity (a), inelastic attenuation (b), and shear-wave anisotropy (c) versus frequency.
The numerical simulations are performed for polar and azimuthal angles of 30°, and two sets of 10-cm-sized identically aligned fractures with density 0.02 , striking 90° and 130° for different saturation fluids (brine, oil, gas).

highest attenuation corresponds to brine, whereas, the attenuation is much lower for oil and practically zero for gas (Figure 9b). For all three fluids, the anisotropy varies with azimuth and is higher for brine and lower for oil and gas (Figure 9c). The anisotropy data suggest a maximum around azimuth of 110–120º. The results undoubtedly reflect the average orientation of the fracture system because the most obvious changes occur at 110–120º, when the two sets of identically aligned fractures strike 90º and 130º. Clearly, velocity and anisotropy are the variables that best distinguish brine from oil and gas. However, anisotropy is the variable that better shows the average orientation of the sets of fractures because the variation maxima for gas or oil are closer to the average orientation of the fractures.

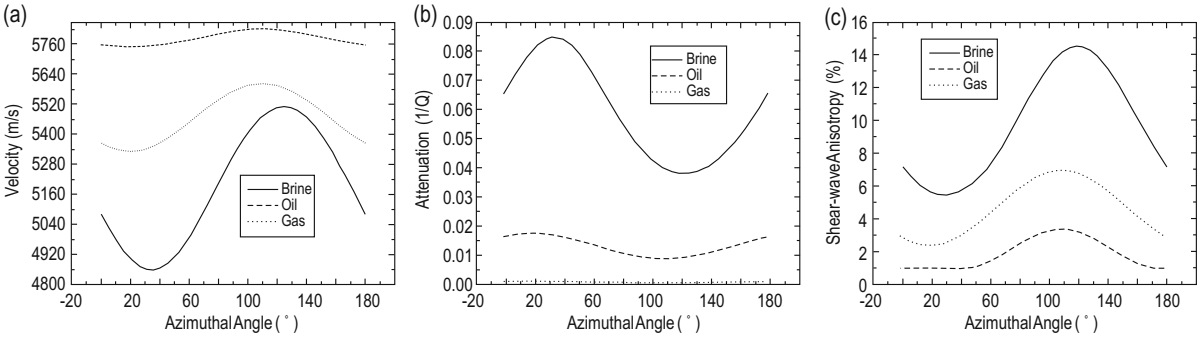

Fig.9 P-wave velocity (a), inelastic attenuation (b), and shear-wave anisotropy (c) versus azimuth.
The numerical simulations are performed for polar angle of 40°, and two sets of 10-cm-sized identically aligned fractures with density of 0.02, striking 90° and 130° for different saturation fluids (brine, oil, gas).

Fracture orientation

Even though one set of fractures has the same strike direction, the P-wave velocity varies with azimuth because of the different orientation of the other set of fractures (Figure 10a). All curves have the same bell shape and the maximum in each one is close to the average direction of the two sets of fractures. The velocity peaks are high, even more when the fracture orientation of both sets are close to each other (70º and 90º) and somewhat less when they differ (30º and 150º). The variation of the attenuation with azimuth is the opposite of that of the velocity (Figure 10b). The anisotropy variation with azimuth is not simple (Figure 10c); however, the anisotropy is high when the fracture directions of both sets are close to each other (70º and 90º). In general, the velocity, attenuation, and anisotropy variations are the highest when the strike orientations of the two sets of fractures coincide or are very close.

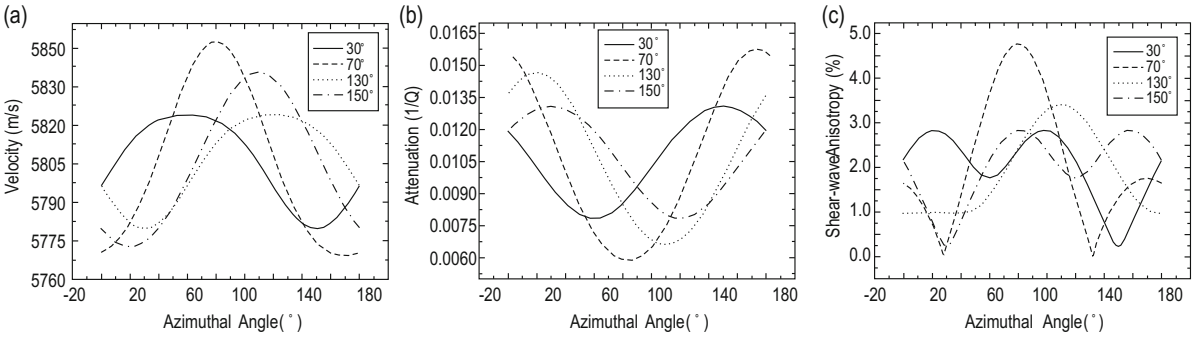

Fig.10 P-wave velocity (a), inelastic attenuation (b), and shear-wave anisotropy (c) versus azimuth.
The numerical simulations are performed for polar angle of 40° and two sets of 10-cm-sized identically aligned fractures, one striking 90° and the other striking at different angles (30°, 70°, 130°, 150°).

Fast-wave polarization angle

Finally, we analyze the effects of density, strike orientation, and size of the two sets of fractures on the fast shear-wave polarization angle (Figure 11). Figure 11a shows the data versus frequency. In the frequency range 0–140 Hz, the fast polarization angle do not

vary much with fequency; they are smaller for lower or null density contrast (1:1) and larger for higher density contrast (1:5). At mid frequencies (140 Hz), the fast-wave polarization angle increases rapidly and progressively reaches almost constant value at high frequencies; however, the polarization angle is larger for lower or null density contrast (1:1) and smaller for higher density contrast (ratio 1:5), and in any case it is greater than the average orientation of the two sets of fractures.

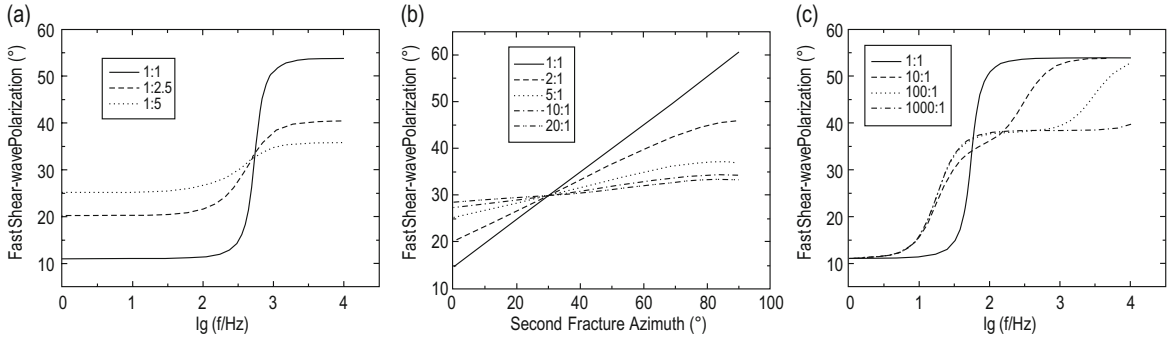

Fig. 11 Fast-wave polarization direction vs (a) density ratios of 1:1, 1:2.5, and 1:5, (b) density ratios of 0.02:0.02, 0.02:0.05, and 0.02:0.1 and strike of 0° to 90°, (c) fracture size ratios of 0.1:0.1, 0.1:0.01, 0.1:0.001, and 1:0.001.
The numerical simulations are performed for polar angle of 40° and two sets of aligned fractures.

The second example deals with the double dependence of the fracture density ratio and azimuth of the second set of fractures. The numerical experiment includes a set of 10-cm-sized identically aligned fractures with fracture density of 0.02 and strike between 0º and 90º, and another identical set of fractures striking 30º and with fracture density of 0.02,0.04,0.1,0.2 and 0.4, respectively, yielding density ratios of 1:1, 2:1, 5:1, 10:1, and 20:1, respectively. The numerical simulations are performed for polar angle of 40º and vertical incident wave. Figure 11b shows that when both sets have the same fracture density ratio (1:1), the fast-wave polarization direction and azimuth are linearly related. A similar effect is observed at density ratios of 2:1 to 20:1), even though the relation is not longer linear. As expected, when the strike direction of the second set of fractures coincides with that of the other set (30º), the fast-wave polarization direction is the same (30º) regardless of the density ratio.

The third example concerns the dependence on fracture size and is for the set of 0.1-m-sized fractures with fracture density 0.02 and 0° strike and another set of equal density and 30º strike but with sizes of 0.1 m, 1 m, 10 m and 100 m, yielding results for size ratios of 1:1, 10:1, 100:1, and 1000:1, respectively. The polar and azimuthal angles are both 30°. Figure 11c shows that at low frequency (<10 Hz) the fracture size has little effect on the fast-wave polarization direction. However, the polarization angle increases quickly as the frequency increases in the range 10–30 Hz, when the fractures differ in size but not so when the fractures are of the same size. At higher frequencies, the fast-wave polarization angle is approximately the same for ratios 100:1 and 1000:1, and greater for ratios 10:1 and 1:1, i.e., when the fracture sizes are closer. Around 600 Hz, the polarization angle begins to differ for ratios of 100:1 and 1:1000. At the highest frequencies, the fast-wave polarization angles corresponding to ratios of 100:1 and 10:1 increase and approach the angle for 1:1, whereas the polarization angle for the higher ratios is around 53º.

Conclusions

Based on the effective medium model proposed by Chapman, we study the effect of fracture-related parameters (size, density, fluid, and strike) on wave propagation in fluid-saturated porous multifractured media. We numerically simulate the variation of the P-wave velocity, attenuation, and shear-wave splitting anisotropy with frequency and azimuth angle of the incident wave.

The results suggest that when the fractures are aligned, the parameters show anisotropy. Compared to one set of fractures, for multiple sets of fracture, velocity, attenuation, and anisotropy shift to higher and wider frequency band range. Different fracture scales have different velocity dispersion and attenuation characteristics. The fracture density has the greatest effect on anisotropy, followed by the fracture size. In

particular, large fracture scales are important at low and middle frequencies. Finally, the type of filling fluids has a strong effect at the low-frequency anisotropy. Compared with velocity and anisotropy, the attenuation dependence on frequency and azimuth angle is clearer but all three can be used to differentiate between open and sealed fractures. The shift of the peaks suggests that the orientations of the two sets of fractures are consistent. When the fracture density is the same, the azimuth at the extremes is the average orientation of the fracture sets. P-wave velocity, attenuation, and anisotropy variations with azimuth can be used to identify the fracture density and scale differences. The P-wave velocity and attenuation (1/Q) with azimuth function has opposite characteristics and the attenuation changes more clearly. Using attenuation, P-wave velocity, and the frequency range of the anisotropy, we can identify the type of filling. If the fractures are similar in size, the fast shear-wave polarization in the middle–low frequency is approximately the average of the fracture orientation with the fracture density as weight. When fracture scale ratios are different, the fast shear-wave polarization depends on frequency. With increasing frequency, the fast shear-wave polarization increases. Therefore, the fast shear-wave polarization of multiple sets of fractures at low frequencies is used to find the main direction of the fracture sets. It is necessary to consider the fracture density, orientation, and scale because these characteristics provide the basis for the detection of fractures in space and time and can be used to identify the type of fluid filling the fractures.

Acknowledgements

This study originated at the suggestion of Professor Zhongjie Zhang (1964–2013), who was the head of department at the Institute of Geology and Geophysics of the Chinese Academy of Sciences (IGGCAS), Beijing. We sincerely thank Professor Tao Xu, a distinguished member of the IGGCAS, for his help and useful advice.

References

Agersborg, R., Johansen, T. A., and Jakobsen, M., 2009, Velocity variations in carbonate rocks due to dual porosity and wave-induced fluid flow, Geophys. Prospect., **57**(1), 81–98.

Aki, K., and Richards, P. G., 1980, Quantitative seismology: Thoery and Method, W.H. Freeman and Company, volume 1.

Batzle, M., Han, D. H., and Hoffmann, R., 2006, Fluid mobility and frequency-dependent seismic velocity - direct measurements: Geophysics, **71**(1), N1–N9.

Borcherdt, R. D., 2009, Viscoelastic waves in layered media: Cambridge University Press.

Cerveny, V., and Psencik, I., 2009, Perturbation Hamiltonians in heterogeneous anisotropic weakly dissipative media: Geophysical Journal International, **178**, 939–949.

Chapman, M., 2003, Frequency dependent anisotropy due to meso-scale fractures in the presence of equant porosity. Geophys. Prospect., **51**(5), 369–379.

Chapman, M., 2009, Modeling the effect of multiple sets of mesoscale fractures in porous on frequency-dependent anisotropy: Geophysics, **74**(6), D97–D103.

Chapman, M., Maultzsch, S., Liu, E., et al., 2003, The effect of fluid saturation in an anisotropic, multi-scale equant porosity model. J. Appl. Geophy., **54**, 191–202.

Carcione, J. M., 2015, Wave fields in real media: Theory and numerical simulation of wave propagation in anisotropic, anelastic, porous and electromagnetic media: Handbook of Geophysical exploration (3rd ed.), Elsevier.

Chen, Z. Q., Zeng, L. B., Huang, P., et al., 2016, The application study of the multi-scales integrated prediction method to fractured reservoir description. Applied Geophysics, 1**3**(1), 80–92.

Crampin, S., 1978, Seismic wave propagation through a cracked solid: polarization as a possible dilatancy diagnostic. Geophs. J. R. astr. Soc., **53**(3), 457–496.

Crampin, S., 1985, Evaluation of anisotropy by shear-wave splitting. Geophysics, **50**, 142–152.

Crampin S., 1994, The fracture criticality of crustal rocks. Geophys. J. Int., **118**, 428–438.

Crampin, S., and Gao, Y., 2014, Two species of microcrack. Applied Geophysics, **11**(1), 1–8.

Fedorov, F. I., 1968. Theory of elastic waves in crystals, Springer.

Guo, G. H., Zhang, Z., Jin, S. X., et al., 2013, Multi-scale fracture and fluid response characteristic in seismic data: Numerical simulation analysis. Chinese J. Geophys., **56**(6), 2002–2011 (in Chinese).

Hao, Q., and He, Q., 2013, A standard linear solid model representation of Chapman's frequency-dependent anisotropy induced by two sets of aligned mesoscale fractures: Journal of Seismic Exploration, **22**, 169–182.

Hao, Q., and Alkhalifah T., 2017, An acoustic eikonal equation for attenuating transversely isotropic media with a vertical symmetry axis: Geophysics, **82**, No.1,

C9–C20.
Hao, Q., and Alkhalifah T., 2017, An acoustic eikonal equation for attenuating orthorhombic media: Geophysics, **82**(4), WA67–WA81.
Hudson, J. A., Liu, E., and Crampin, S., 1996, The mechanical properties of materials with interconnected cracks and pores. Geophys. J. Int., **124**, 105–112.
Jakobsen, M., 2004, The interacting inclusion model of wave induced fluid flow. Geophys. J. Int., **158**, 1168–1176.
Kraut, E. A., 1963, Advances in the theory of aniosotropic elastic wave propagation. Rev. Geophys., **1**, 401–408.
Liu, E., Crampin, S., Queen, J. H., et al., 1993, Behaviour of shear-waves in rocks with two sets of parallel cracks. Geophys. J. Int., **113**, 509–517.
Liu, E., Hudson, J. A., Pointer T., 2000, Equivalent medium representation of fractured rock. J. Geophys. Res., **105**(B2), 2981–3000.
Liu, K., Zhang, Z. J., Hu, J. F., et al., 2001, Frequency band dependence of S-wave splitting in China mainland and its implications. Science in China (Series D), **31**(2), 155–162.
Liu, E. R., Yue, J. H., and Pan, D. M., 2006, Frequency-dependent anisotropy: Effects of multiple fracture sets on shear-wave polarizations. Chinese J. Geophys., **49**(5), 1401–1409 (in Chinese).
Liu, E. R., Chapman, M., Zhang, Z. J., and Queen, J. H., 2006, Frequency-dependent anisotropy: Effects of multiple fracture sets on shear polarizations. Wave Motion, **44**, 44–57.
Liu, Y. Y., 2012, Studying on the response of seismic waves in medium with multiple sets of multi-scale fractures. MSc Thesis, China University of Geosciences, Beijing.
Maultzsch, S., Chapman, M., Liu, E., et al., 2003, Modelling frequency-dependent seismic anisotropy in fluid-saturated rock with aligned fractures: implication of fracture size estimation from anisotropic measurements. Geophys. Prospect., **51**(5), 381–392.
Maultzsch, S., Chapman, M., Liu, E., and Li, X. Y., 2007a, Observation of anisotropic attenuation in VSP data. Journal of Seismic Exploration, **16**, 2–4, 145–158.
Maultzsch, S., Chapman, M., Liu, E., and Li, X. Y., 2007b, Modeling and analysis of attenuation in multiazimuth VSP data from the Clair field. Geophys. Prospect., **55**, 627–642.
Park-Nolte, L. J., and Nolte, D. D., 1992, Frequency dependence of fracture stiffness. Geophys. Res. Lett., **19**(3), 325–328.
Pointer, T., Liu, E., and Hudson, J. A., 2000, Seismic wave propagation in cracked porous media. Geophys. J. Int., **142**, 199–231.
Schoenberg, M., Dean, S., and Sayers, C. M., 1999, Azimuthal-dependent turning of seismic waves reflected from fractured reservoirs. Geophysics, **64**(4), 1160–1171.
Shi, S. H., 2007, Dependency relationship of fracture size, anisotropy and frequency in HTI media based on developing equivalent media model. PhD. Thesis, Jilin University, China.
Wei, X. C., Lu, M. H., Ba, J., et al., 2008, Dispersion and attenuation of elastic waves in a viscous fluid-saturated anisotropic porous solid. Chinese Journal of Geophysics, **51**(1), 213–220.

Appendix A

The frequency-dependent elastic parameters are from Chapman (2003, 2009). The fracture densities ε_1 and ε_2, fracture scales a_{f1} and a_{f2} , and scale factor τ_f are also defined by Chapman (2003, 2009) as

$$\tau_f = \frac{8l(1-\upsilon))(1+K_c)}{3\mu}\left(\frac{\eta}{k}\right)a_f, \tag{A-1}$$

where η is the pore fluid viscosity, k is the permeability, υ is Poisson's ratio, λ and μ are the Lamé parameters of the background medium, and k_f is the fluid bulk modulus. The notation used is

$$\sigma_c = \frac{\pi\mu a_f}{2(1-\upsilon)}, \tag{A-2}$$

$$K_c = \frac{\sigma_c}{k_f}, \tag{A-3}$$

$$K_p = \frac{4\mu}{3k_f}, \tag{A-4}$$

$$S_{ij}^1(\omega) = \frac{i\omega\tau_1 n_i^1 n_j^1}{(1+i\omega\tau_1)(1+K_c^1)}, \tag{A-5}$$

$$S_{ij}^2(\omega)=\frac{i\omega\tau_2 n_i^2 n_j^2}{(1+i\omega\tau_2)(1+K_c^2)}, \tag{A-6}$$

where n is the unit vector normal to the fracture plane, superscripts 1 and 2 refer to the first and second set of fractures, τ is the fracture scale factor, and ω is the angular frequency. Then, if

$$F_1(\omega)=\frac{1}{1+i\omega\tau_1}, \tag{A-7}$$

$$F_2(\omega)=\frac{1}{1+i\omega\tau_2}, \tag{A-8}$$

the fluid pressure in pores is

$$p^{*}=H_{ij}^3(\omega)\sigma_{ij} \tag{A-9}$$

and

$$H_{ij}^3(\omega)=\frac{\frac{\varphi_1^0}{\sigma_c^1}[n_i^1 n_j^1-(1+K_c^1)S_{ij}^1(\omega)]+\frac{\varphi_2^0}{\sigma_c^2}[n_i^2 n_j^2-(1+K_c^2)S_{ij}^2(\omega)]+\frac{3\varphi_p^0}{4\mu}\frac{1-\upsilon}{1+\upsilon}\delta_{ij}}{\frac{\varphi_1^0}{\sigma_c^1}(1+K_c^1)F_1(\omega)+\frac{\varphi_2^0}{\sigma_c^2}(1+K_c^2)F_2(\omega)+\frac{3\varphi_p^0}{4\mu}(1+K_p)}, \tag{A-10}$$

where φ with the subscripts suggests the percentage of volume of fluid in pores or fractures, subscript p refers to the pores, and subscripts 1 and 2 reference to the set of fractures.

Similarly, the pressure in the two sets of fractures is

$$f_1=H_{ij}^1(\omega)\sigma_{ij}, \tag{A-11}$$

$$f_2=H_{ij}^2(\omega)\sigma_{ij}, \tag{A-12}$$

where

$$H_{ij}^1(\omega)=S_{ij}^1(\omega)+F_1(\omega)H_{ij}^3(\omega), \tag{A-13}$$

$$H_{ij}^2(\omega)=S_{ij}^2(\omega)+F_2(\omega)H_{ij}^3(\omega). \tag{A-14}$$

Chapman calculated the frequency-dependent effective elastic tensor using the equation (Eshelby, 1957)

$$C_{ijkl}\varepsilon_{ij}^0\varepsilon_{kl}^0=C_{ijkl}^m\varepsilon_{ij}^0\varepsilon_{kl}^0-\sum_n\varphi_n(\varepsilon_{ij}^{inc}\sigma_{ij}^0-\sigma_{ij}^{inc}\varepsilon_{ij}^0), \tag{A-15}$$

where superscript 0 denotes the elastic tensor of the background medium, C_{ijkl}^m is the elastic tensor of the rock frame, and superscript *inc* refers to the elastic inclusions within each empty space. In the case of two sets of fractures, particular stress σ^0 and strain ε^0 values with respect to the fracture orientation are chosen to isolate the five independent components of the elastic tensor ε^0. The method leads to the frequency-dependent elastic tensor (Chapman, 2009)

$$C_{ijkl}(\omega)=C_{ijkl}^m-\varphi C_{ijkl}^p(\omega)-\varepsilon_1 C_{ijkl}^{f1}(\omega)-\varepsilon_2 C_{ijkl}^{f2}(\omega). \tag{A-16}$$

Defining the strike angle θ_m and the inclination angle φ_m of the m-th set of fractures in the normal direction, we obtain

$$n^m=(\cos\theta_m\sin\varphi_m,\sin\theta_m\sin\varphi_m,\cos\varphi_m), \tag{A-17}$$

and the rotation matrix is

$$R_{ij}^m(\theta_m,\varphi_m)=\begin{bmatrix}\cos\theta_m\cos\varphi_m & -\sin\theta_m & \cos\theta_m\sin\varphi_m\\ \sin\theta_m\cos\varphi_m & \cos\theta_m & \sin\theta_m\sin\varphi_m\\ -\sin\varphi_m & 0 & \cos\varphi_m\end{bmatrix}. \tag{A-18}$$

A set of stress tensors is chosen

$$\sigma_{ij}^1=\begin{bmatrix}\lambda+2\mu & 0 & 0\\ 0 & \lambda & 0\\ 0 & 0 & \lambda\end{bmatrix}, \tag{A-19}$$

$$\sigma_{ij}^2=\begin{bmatrix}\lambda & 0 & 0\\ 0 & \lambda & 0\\ 0 & 0 & \lambda+2\mu\end{bmatrix}, \tag{A-20}$$

$$\sigma_{ij}^{3}=\begin{bmatrix}2(\lambda+\mu) & 0 & 0\\ 0 & 2(\lambda+\mu) & 0\\ 0 & 0 & 2\lambda\end{bmatrix}, \quad \text{(A-21)}$$

$$\sigma_{ij}^{4}=\begin{bmatrix}2(\lambda+\mu) & 0 & 0\\ 0 & 2\lambda & 0\\ 0 & 0 & 2(\lambda+\mu)\end{bmatrix}. \quad \text{(A-22)}$$

Each of these tensors is used as the stress field σ_{ij}^{0} at infinity; this form is chosen to make easier the separation of the various components of the fracture tensors. The fluid pressure is

$$f_m^p = H_{ij}^m R_{ia}^m R_{jb}^m \sigma_{ab}^p, \quad (m = 1, 2;\ \ p = 1, 2, 3, 4) \quad \text{(A-23)}$$

and we obtain the following expressions

$$a_{11}^m = \varphi_m^0\left[\frac{\lambda}{\sigma_c^m}(\lambda - f_m^1) - f_m^1\right], \quad \text{(A-24)}$$

$$a_{33}^m = \varphi_m^0\left[\frac{\lambda+2\mu}{\sigma_c^m}(\lambda+2\mu - f_m^2) - f_m^2\right], \quad \text{(A-25)}$$

$$a_{12}^m = \varphi_m^0\left[\frac{\lambda}{\sigma_c^m}(2\lambda - f_m^3) - f_m^3\right] - \frac{1}{2}(a_{11}^m + a_{33}^m), \quad \text{(A-26)}$$

$$a_{12}^m = \varphi_m^0\left[\frac{\lambda}{\sigma_c^m}(2\lambda - f_m^3) - f_m^3\right] - \frac{1}{2}(a_{11}^m + a_{33}^m), \quad \text{(A-27)}$$

$$a_{55}^m = \varphi_m^0\frac{4\mu(1-\upsilon)}{\pi(2-\upsilon)r_m}, \quad \text{(A-28)}$$

$$\begin{bmatrix}a_{11}^m & a_{12}^m & a_{13}^m & 0 & 0 & 0\\ a_{12}^m & a_{11}^m & a_{13}^m & 0 & 0 & 0\\ a_{13}^m & a_{13}^m & a_{33}^m & 0 & 0 & 0\\ 0 & 0 & 0 & a_{55}^m & 0 & 0\\ 0 & 0 & 0 & 0 & a_{55}^m & 0\\ 0 & 0 & 0 & 0 & 0 & 0\end{bmatrix}, \quad \text{(A-29)}$$

that are used to calculate the elastic correction term.

The stress tensor in standard matrix form is

$$\sigma_{ij}^{5}=\begin{bmatrix}3\lambda+2\mu & 0 & 0\\ 0 & 3\lambda+2\mu & 0\\ 0 & 0 & 3\lambda+2\mu\end{bmatrix}, \quad \text{(A-30)}$$

and the pore fluid pressure is

$$p^* = H_{ij}^3\sigma_{ij}^5. \quad \text{(A-31)}$$

Thus, the pore elastic correction is

$$d = \varphi\left[\frac{3\lambda+4\mu}{12\mu}\left(\frac{1-\upsilon}{1+\upsilon}\sigma_{ll}^5 - p^*\right) - \frac{1}{3}p^*\right], \quad \text{(A-32)}$$

$$e = \varphi 15\mu\frac{1-\upsilon}{7-5\upsilon}, \quad \text{(A-33)}$$

and the standard matrix form of the tensor $C_{ijkl}^p(\omega)$ owing to pore pressure is

$$\begin{bmatrix}\left(d+\frac{4}{3}e\right) & \left(d-\frac{2}{3}e\right) & \left(d-\frac{2}{3}e\right) & 0 & 0 & 0\\ \left(d-\frac{2}{3}e\right) & \left(d+\frac{4}{3}e\right) & \left(d-\frac{2}{3}e\right) & 0 & 0 & 0\\ \left(d-\frac{2}{3}e\right) & \left(d-\frac{2}{3}e\right) & \left(d+\frac{4}{3}e\right) & 0 & 0 & 0\\ 0 & 0 & 0 & e & 0 & 0\\ 0 & 0 & 0 & 0 & e & 0\\ 0 & 0 & 0 & 0 & 0 & e\end{bmatrix}. \quad \text{(A-34)}$$

The effective frequency-dependent elastic tensor is the sum of the elastic tensor of the background medium, the pore correction, and the correction for the two sets of fractures in the material coordinate system

$$C_{ijkl}(\omega) = C_{ijkl}^0 - C_{ijkl}^p(\omega) - \sum_{m=1}^{2} R_{ip}^m R_{jq}^m R_{kr}^m R_{ls}^m a_{pqrs}^m. \quad \text{(A-35)}$$

Guo Gui-Hong, graduated in 1998 by the Changchun Science and Technology University with a Bachelor Degree in oil and gas exploration. Ph.D. in Geophysics in 2007, Institute of Geology, China Earthquake Administration. At present, she is working as associate professor and researcher in the Department of Geology Engineering, Lanzhou University. Her current research includes seismology and seismic exploration.